Hindawi
Shock and Vibration
Volume 2022, Article ID 4066950, 15 pages
https://doi.org/10.1155/2022/4066950

Research Article

Air Waves Induced by Truck Passage in a Slender Motorway

Fabio Rizzo,[1] **Aleksander Pistol**,[2] **Alberto Viskovic**,[3] **and Marco Petrangeli**[3]

[1]*Cracow University of Technology, Chair of Metal Structure L-3, Department of Civil Engineering, Krakow, Poland*
[2]*Cracow University of Technology, Wind Engineering Laboratory, Kraków, Poland*
[3]*G. D'Annunzio University of Chieti-Pescara, viale Pindaro 42, Pescara, Italy*

Correspondence should be addressed to Fabio Rizzo; fabio.rizzo@universityresearch.it

Received 22 February 2022; Accepted 4 May 2022; Published 20 May 2022

Academic Editor: Sandro Carbonari

The interaction between a pedestrian bridge for a motorway crossing and air pressure waves induced by the truck passage is discussed with reference to a slender footbridge in Pregnana (Italy). The experimental campaign was necessary, as very significant vibrations induced by truck passage were observed during the construction process before building the reinforced concrete plate on the deck. Results obtained from monitoring the air pressures and accelerations caused by the truck passage under the bridge along with truck speeds have shown a phenomenon known as a piston effect occurring during the passage. Based on the statistical analysis of these measured values, the spatial distribution of the wave on the bridge was elaborated. Numerical analyses of the bridge without the reinforced concrete plate on the deck suggest that the piston effect should be calculated to safely construct light bridges.

1. Introduction

In highly congested motorways, trucks usually travel at constant speed and spacing, creating a pulsating effect that can lead to significant vibrations in overpasses. The pressure waves created by truck passage lose very little energy before buffeting the deck because overpasses are generally placed as close as possible to the minimum required vertical clearance and large trucks use most of the available clearance. These air pressure waves can be particularly harmful if the overpass structure is light [1], in which case the structure-wave interaction may even affect the structural safety. This phenomenon becomes particularly significant when two large trucks move at high speeds one after another under a motorway crossing [2, 3]. Few studies discuss this phenomenon, and the vast majority investigates the air wave induced by trucks through CFD as for example, Bojanowski et al. [2].

The consequence is a phenomenon known as the *piston effect* that applies a high pressure on the bridge structure and may induce significant structural vibration [4, 5], particularly if the frequency of the air pressure wave excitation is close to one of the natural frequencies of the bridge. However, few studies discuss the interaction between brigs and truck passage while many more discuss the piston effect induced by the train passage, for example, Pan et al. [5] gave a review of the piston effect in subway stations.

The effects of this structure-wave interaction are likely to become more common and harmful, as the demand for light structures increases. However, this phenomenon is largely neglected in modern bridge design codes, where no information is given regarding the relationships between the sizes of the structures, natural frequencies, and air wave effects. With the exception of Bojanowski et al. [2], there is a large scientific gap in the topic of the interaction between overpasses and truck traffic-induced air wave pressure, whereas there is focus on effects caused by wind instability and fatigue collapse of cantilevered overhead sign structures. Creamer et al. [6] described the results of an experimental and analytical study to determine fatigue loading on cantilever highway signs caused by gusts produced by trucks passing under the sign. Three actual sign structures were instrumented in-field to determine their response to gusts caused by the trucks. Results showed that, for the cases considered in the study, the low stress levels measured in the superstructure did not indicate potential fatigue problems. Johns and Dexter [7] presented a procedure to calculate fatigue design load ranges for signs and signal support

(a) (b)

Figure 1: Pregnana footbridge: (a) in-service overpass on the TO-MI highway; (b) preassembly of steel beams and deck for the main span.

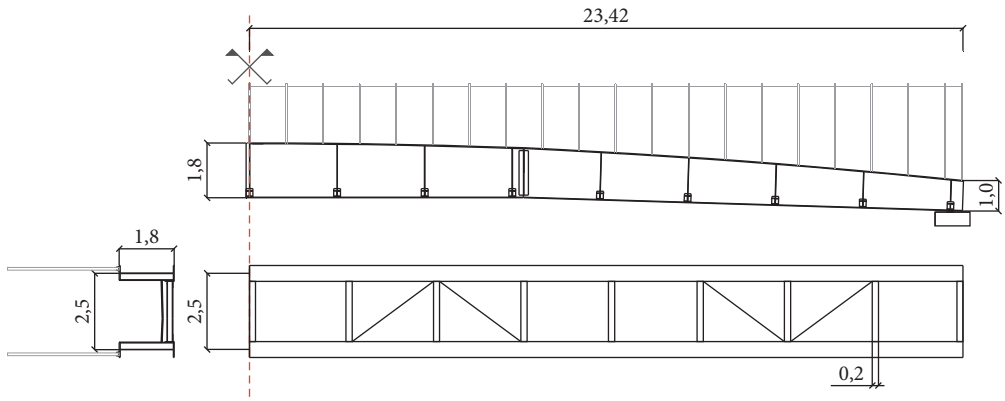

Figure 2: Side view (upper drawing), transverse cross-section (left), and plan view from below of the Pregnana bridge.

structures. Wind-tunnel experiments were conducted to calculate the equivalent static fatigue limit-state load range induced by the three wind-loading phenomena: galloping, natural wind gusts, and truck-induced wind gusts. Gallow [8] reported several cases of fatigue-related failures of cantilevered overhead sign structures due to truck-induced wind gusts. It also confirmed that resonance occurs when the frequency of wind gust loads matches the fundamental frequency of the structure and consequently that fatigue stresses increase and may exceed the critical fatigue limit, resulting in failure.

The scientific literature mentioned above suggests that flexible structures are sensitive to the airwave induced by the trucks passage and that resonance and fatigue can affect the structure reliability. Based on this consideration, this paper aims to investigate the interaction between air waves induced by truck passage and overpasses for a specific case study discussing the spatial propagation of the wave on the bridge. The case study considered here is the Pregnana footbridge over the Milan-Turin (MI-TO) motorway in Italy.

2. The Prototype Architecture

The case study considered in this paper is one of the 21 pedestrian and bicycle crossings along the Turin-Milan motorway in Italy. 19 of these crossings are underpasses and the remaining two are overpasses. The two pedestrian bridges were initially designed as two classic extradosed truss girders with top and bottom bracings. This structurally efficient solution, however, would have not been equally efficient from a maintenance point of view, as this can induce corrosion [9–11]. For this reason, the original project was modified and an open "U" section was built. Two longitudinal double T girders connected by transversal beams made the bridge section. The Pregnana footbridge is made with tapered beams that have a shallow arch shape, as shown in Figures 1(a) and 1(b). Beam height varies from 1.0 m at the supports to 1.80 m at midspan. The span between supports is 46 m, and the pedestrian path is 2.50 m wide. A safety and lighting net with a maximum height of 4 m was also added to the bridge. The two main beams are connected by transverse beams of HEA200 profile supporting a corrugated steel sheet deck (HIBOND) connected with a concrete slab (12 cm of thickness in total). The minimum clearance from the motorway level up to the intrados of the bridge is 5.50 m.

Figure 2 shows the plane, front, and back view of the bridge and provides the structural sizes and components. Supports are made of simple rubber pads with a thickness (height) of 10 cm to accommodate for thermal expansion/contraction of the girder.

The Pregnana footbridge was assembled on-site and hoisted in place during a nighttime closure in 2008. The bridge was initially placed without the concrete slab and without the final bituminous surfacing and started to vibrate

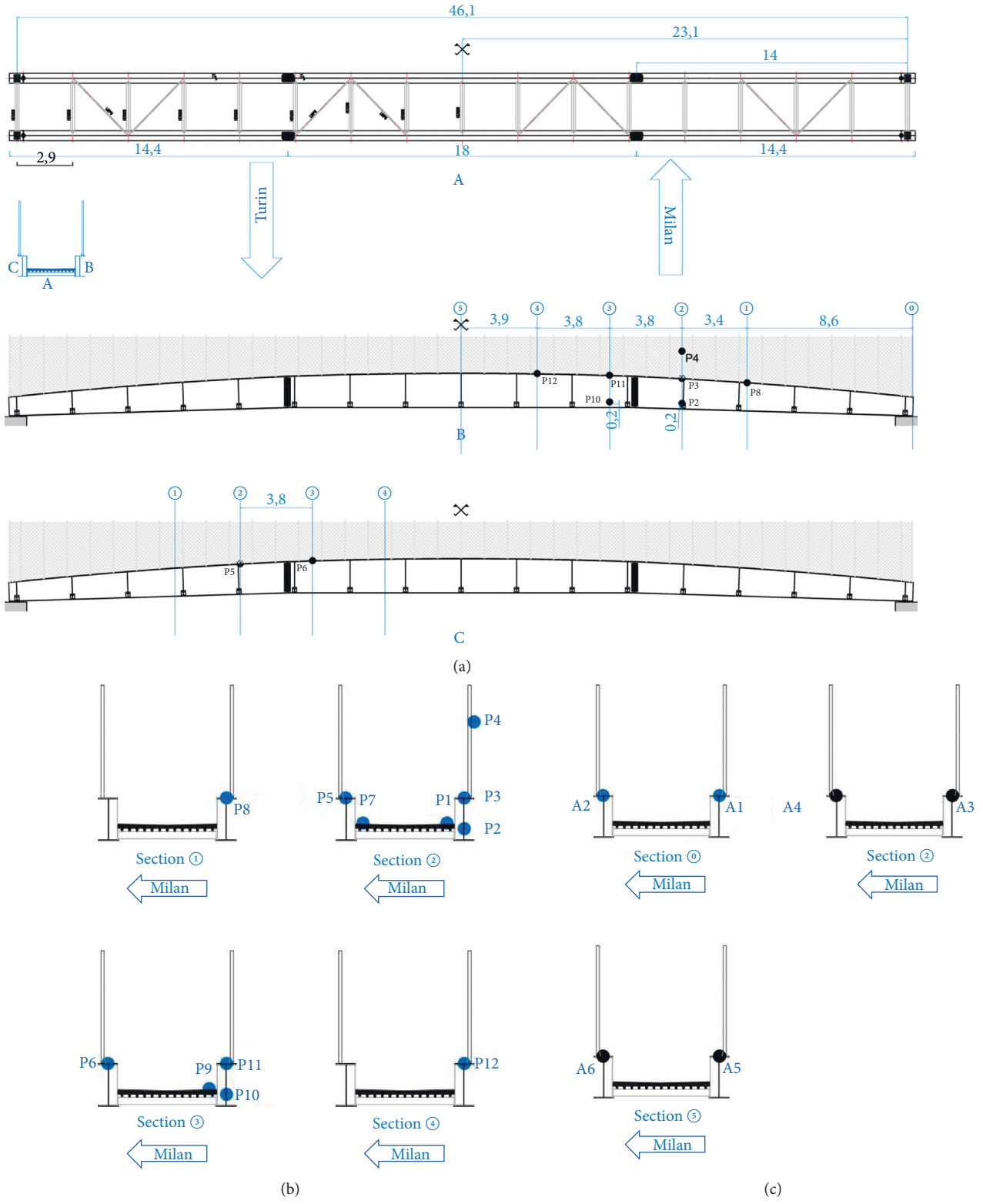

FIGURE 3: (a, b) Positions of pressure sensors in the cross-sections; (c) position of accelerometers A1-A6. In picture (c) Section (0) corresponds to a cross section in the bridge supports.

alarmingly because of the air pressure wave generated by trucks passage immediately after erection and subsequent reopening of that stretch of motorway. This vibration reduced significantly after the concrete deck construction. However, the issue was considered worth of further investigation and a monitoring campaign was started.

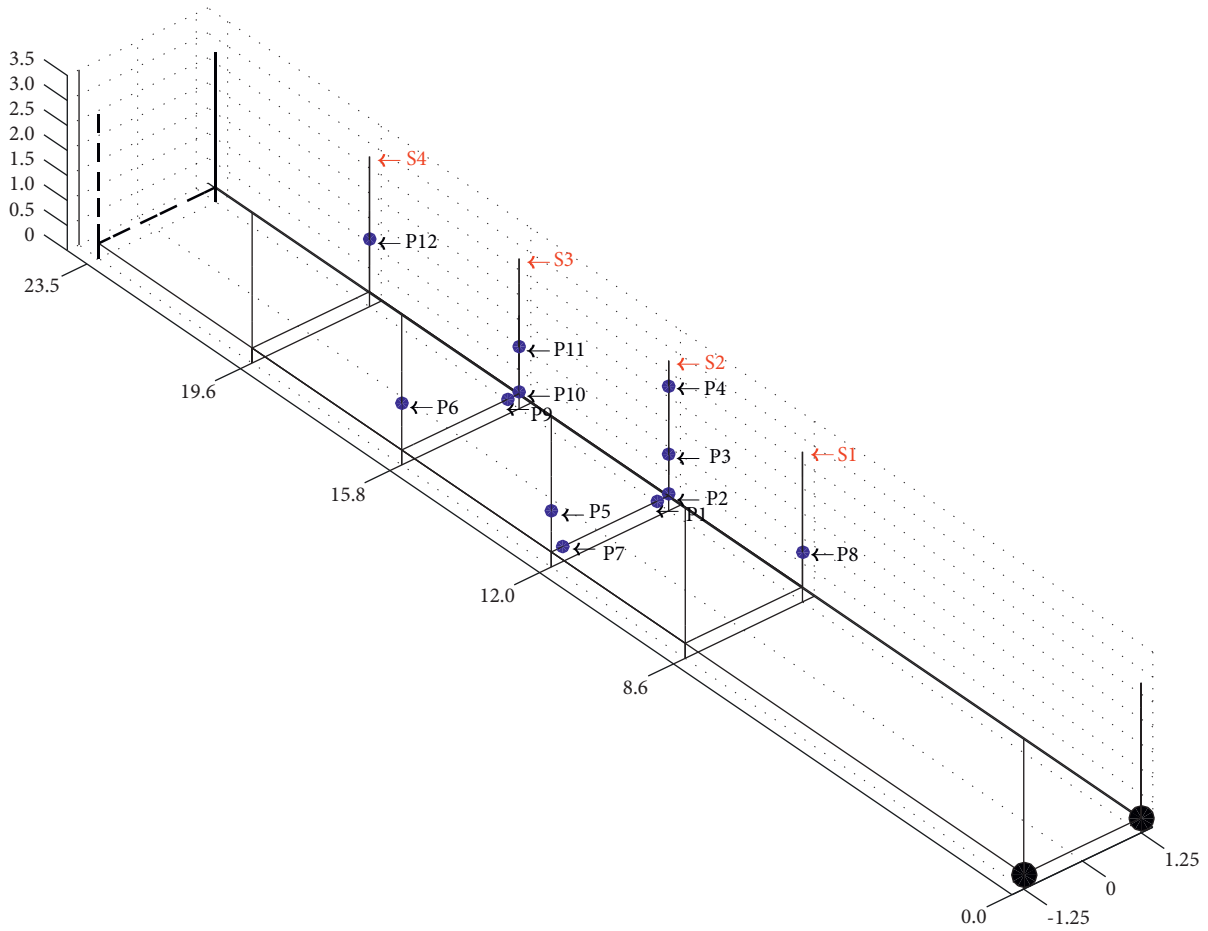

Figure 4: Pressure taps (from P1 to P12) setup.

3. Experimental Campaign Setup

A monitoring campaign was carried out to investigate the effect induced by truck passage with a speed bigger than 80 km/h. In total, twelve pressure sensors (Figures 3 and 4) and 6 accelerometers (Figures 3 and 5) were used for monitoring the bridge. The accelerometers were located at midspan, at the support and at $L/4$ (where L is the footbridge span). Moreover, 4 photoelectric cells were installed to active the measurements of the trucks speed. The pressure sensors had a working pressure of 1.25 kPa with a precision of ±5 inch H_2O and a pressure limit of 34.7 kPa.

The sensors sensitivity was equal to 4000 V/kPa, and they were calibrated before the experiment. A data acquisition system made of 32 analog channels was used for pressure and accelerometer signals, four digital channels received truck speed signals, and one serial channel acquired temperature and air humidity measurements. Signals were acquired with a sampling frequency of 200 Hz for a duration of 120 s [10, 11] each 30 minutes for 3 hours a day and for 5 days. For sake of brevity, only the most significant acquisition is discussed in this paper.

The used accelerometers were Brüel & Kjær Delta Tron 4507B006 cubic models. They were unidirectional vertical (A1, A3, and A5) and horizontal (A2, A4, and A6). The max acceleration was 14 g, shock acceleration was 5000 g, and sensitivity was 500 mV/g. The accelerometer resonance frequency was 18 kiloHz.

4. Results Analysis and Discussion

4.1. Pressure Fields and the Truck Passage-Induced Wave Spatial Distribution. Table 1 reports the positive (pressure) and negative (suction) extreme values (i.e., statistic maxima and minima) and the standard deviations of the pressure measurements. The largest negative and positive pressure values were recorded at pressure sensor P9, and the recorded time history is illustrated in Figure 6. Pressure taps P1, P7, and P9 measured the pressure under the deck, so positive values mean upward action. The upwind pressure sensors were P2, P3, P4, P8, P10, P11, and P12, and the downwind ones were P5 and P6.

The measured pressure time histories were normalized (by subtracting the mean and diving the result by the standard deviation) in order to evaluate their positive ($g_{T_{0,p}}$) and negative peak factors ($g_{T_{0,n}}$). Values are listed in Table 2, and they range from 3.32 (in P5) to 6.97 (in P4). Table 2 also gives the skewness coefficient, γ_{c_p}, and the excess kurtosis, κ_{c_p}.

It can be observed that most of the measured pressure time histories (with the exception of those measured at pressure taps P5 and P6) have a difference of at least 1.0 between the skewness coefficient and the excess kurtosis with

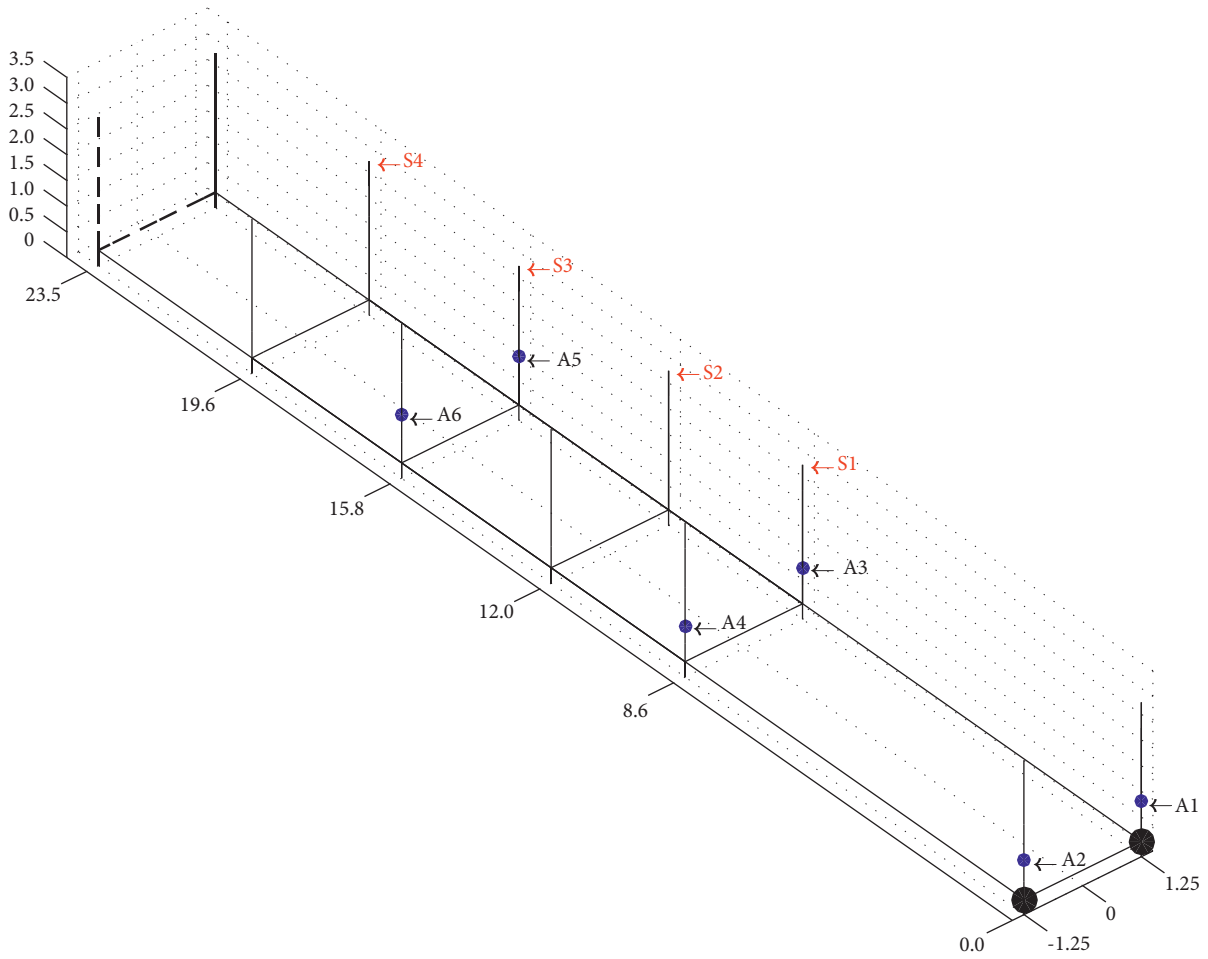

Figure 5: Accelerometers (from A1 to A6) setup.

Table 1: Maximum and minimum values recorded by pressure transducers.

Section	Sensor	Acquisition						$\overline{P}$	σ
		1	2	3	4	5	6		
		kPa						kPa	
S1	P8	0.046	0.049	0.031	0.038	0.034	0.055	−0.025	0.011
S2	P1	0.032	0.063	0.078	0.061	0.086	0.026	0.042	0.009
	P2	0.053	0.048	0.091	0.083	0.070	0.038	0.058	0.024
	P3	0.040	0.042	0.080	0.079	0.053	0.030	0.064	0.021
	P4	0.047	0.026	0.041	0.038	0.042	0.025	0.054	0.021
	P5	−0.028	−0.027	−0.024	−0.026	−0.024	−0.019	0.037	0.009
	P7	−0.036	−0.056	−0.130	−0.085	−0.088	−0.067	−0.077	0.032
S3	P6	−0.017	−0.045	−0.018	−0.018	−0.023	−0.027	−0.025	0.003
	P9	0.061	0.052	0.048	0.044	0.052	0.043	0.050	0.007
	P10	0.053	0.048	0.056	0.089	0.052	0.049	0.058	0.016
	P11	0.040	0.038	0.042	0.076	0.040	0.040	0.046	0.015
S4	P12	0.032	0.028	0.030	0.034	0.061	0.045	0.038	0.013

an absolute value larger than 0.5, which is the conventional value suggested in [12] above which the pressure coefficient process can be considered non-Gaussian. These results suggest that the upwind side (pressure taps P2, P3, P4, P8, P10, P11, and P12) and the bottom (pressure taps P1, P7, and P9) of the bridge are subjected to non-Gaussian pressure processes, whereas the downwind side (pressure taps P5 and P6) is subject to (approximately) Gaussian pressure processes.

Figure 7 shows the time history of the lift (L) force that ranges from −0.1 to 0.15 kPa obtained by summing P2, P3,

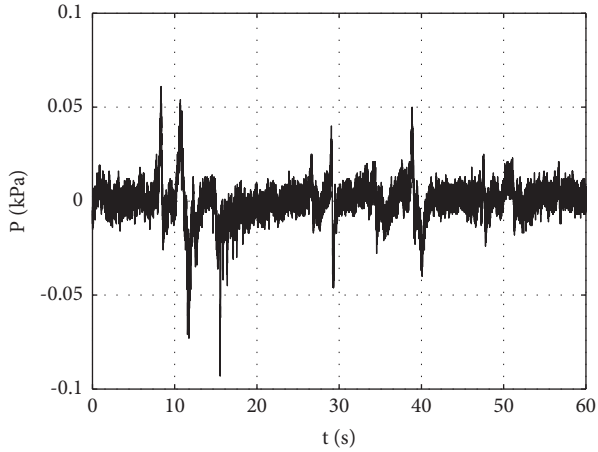

Figure 6: Pressure time history at P9 (S3).

Table 2: Peak factors and higher-order statistics of the measured pressure coefficients.

	P1	P2	P3	P4	P5	P6	P7	P8	P9	P10	P11	P12
$g_{T_{,p}}$	4.36	5.34	4.49	6.97	3.32	4.02	3.77	6.88	5.71	5.87	5.16	4.66
$g_{T_{,n}}$	4.63	3.83	4.94	4.89	4.90	3.25	5.02	5.69	8.71	6.31	4.38	7.57
γ_{c_p}	0.24	0.47	0.33	0.13	0.04	0.07	−0.67	0.52	−0.58	0.09	0.19	−0.17
κ_{c_p}	−0.67	0.99	0.76	0.72	−0.16	0.05	1.67	2.25	7.47	2.20	1.18	3.33

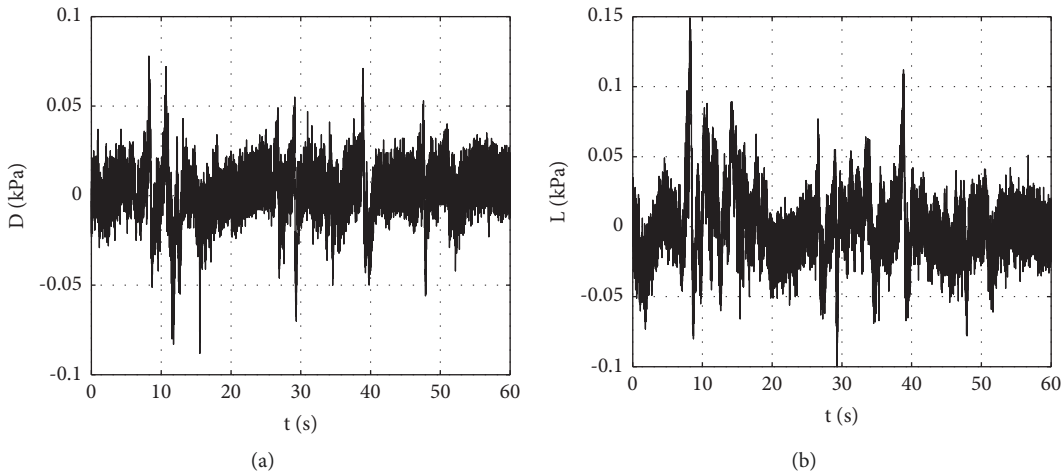

Figure 7: Drag (a) and lift (b).

P4, P5, P6, P8, P10, P11, and P12 values and the time history of the drag (D) force that ranges from −0.08 to 0.07 kPa (kPa), obtained by summing P1, P7, and P9 values.

Figures 8(a) and 8(c) show the pressure envelope in Pa against the truck passage direction, and Figures 8(b) and 8(d) show the pressure envelope in the same direction of the truck passage, in Sections S2 and S3, respectively. Finally, Figure 8(e) shows the pressure envelope on the top and bottom surfaces of the bridge deck. It was observed that the pressure distribution measured in this experimental campaign is qualitatively very similar to the design load conditions recommended for the train passage under bridges by the Italian Railroad Network technical report in 2005 [13].

To give a more synthetic overview of spatial wave distribution, the recorded pressure were analyzed by the singular value decomposition (SVD). In linear algebra, the SVD of a matrix is a factorization of that matrix into three matrices, which have interesting algebraic properties and convey important geometrical and theoretical insights about

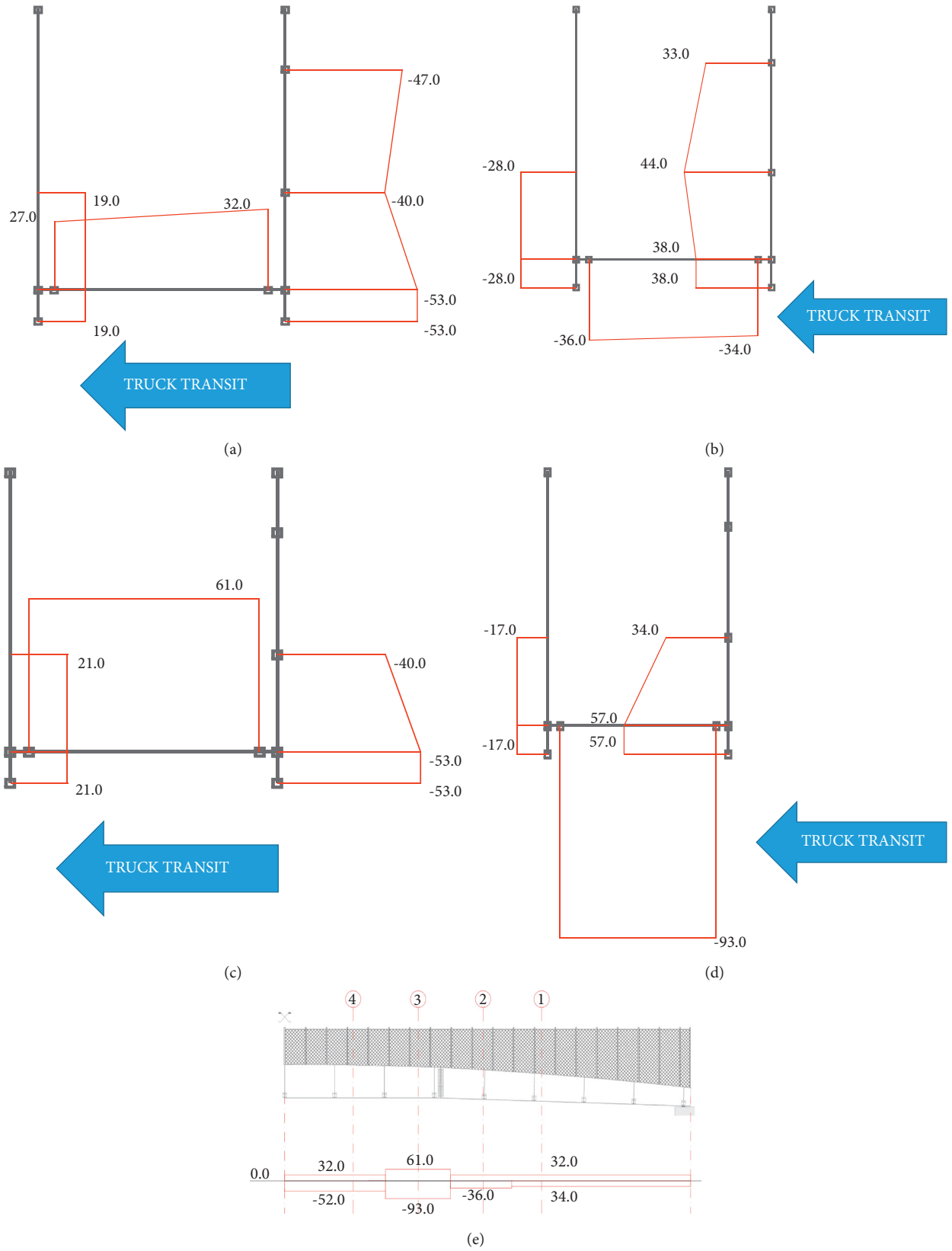

FIGURE 8: Pressure envelope in Pa in the opposite (a, c) and in the same (b, d) direction of the truck passage, in Section S2 (a, b) and Section S3 (c, d); upward and downward pressure envelope on the deck (e).

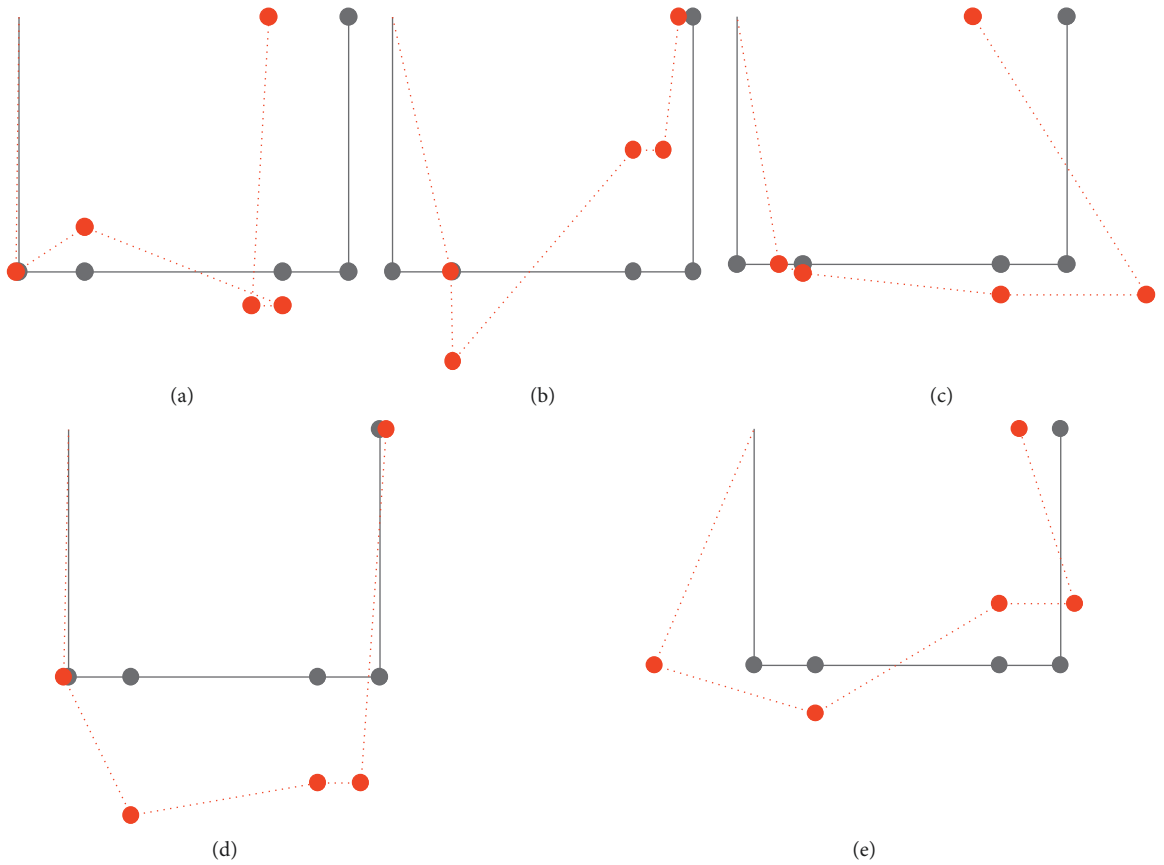

Figure 9: Pressure modes form 1 (a) to 5 (e).

Table 3: Normalized kinetic energy of pressure modes.

Pressure taps	Modes				
	1th	2th	3th	4th	5th
P1	0.06	0.37	0.02	0.17	0.03
P2	0.90	0.05	0.22	0.01	0.00
P3	0.61	0.01	0.31	0.00	0.02
P5	0.00	0.20	0.06	0.00	0.13
P7	0.10	0.20	0.00	0.30	0.02

linear transformations. This method also has important applications in data science [14]. Singular value decomposition takes a rectangular matrix of gene expression data (defined as A, where A is a $n \times p$ matrix) in which the n rows represent the genes, and the p columns represent the experimental conditions. The SVD theorem states:

$$A_{n\times p} = U_{n\times n} \times S_{n\times p} \times V^T_{p\times p}, \quad (1)$$

where the $U_{n\times n}$ columns are the left singular vectors (gene coefficient vectors), $S_{n\times p}$ (the same dimensions as A) has singular values and is diagonal (mode amplitudes), and $V^T_{p\times p}$ has rows that are the right singular vectors (expression level vectors). The SVD represents an expansion of the original data in a coordinate system where the covariance matrix is diagonal. Calculating the SVD consists of finding the eigenvalues and eigenvectors of $A_{n\times p} \times A^T_{n\times p}$ and $A^T_{n\times p} \times A_{n\times p}$. The eigenvectors of $A^T_{n\times p} \times A_{n\times p}$ make up the columns of $V_{p\times p}$, and the eigenvectors of $A_{n\times p} \times A^T_{n\times p}$ make up the columns of $U_{n\times p}$. The singular values in $S_{n\times p}$ are also square roots of eigenvalues from $A_{n\times p} \times A^T_{n\times p}$ or $A^T_{n\times p} \times A_{n\times p}$. The singular values are the diagonal entries of the $S_{n\times p}$ matrix and are arranged in descending order. The singular values are always real numbers. If matrix $A_{n\times p}$ is a real matrix, then, $U_{n\times n}$ and $V_{p\times p}$ are also real.

Figure 9 shows the five pressure modes ordered for decreasing kinetic energy content estimated from records in Section S2 (Figure 4).

The normalized kinetic energy associated to each pressure mode for all pressure sensors in section S2 (Figure 4) is listed in Table 3. It was observed that the most relevant mode for pressure taps P1 and P5 is the second one, whereas for

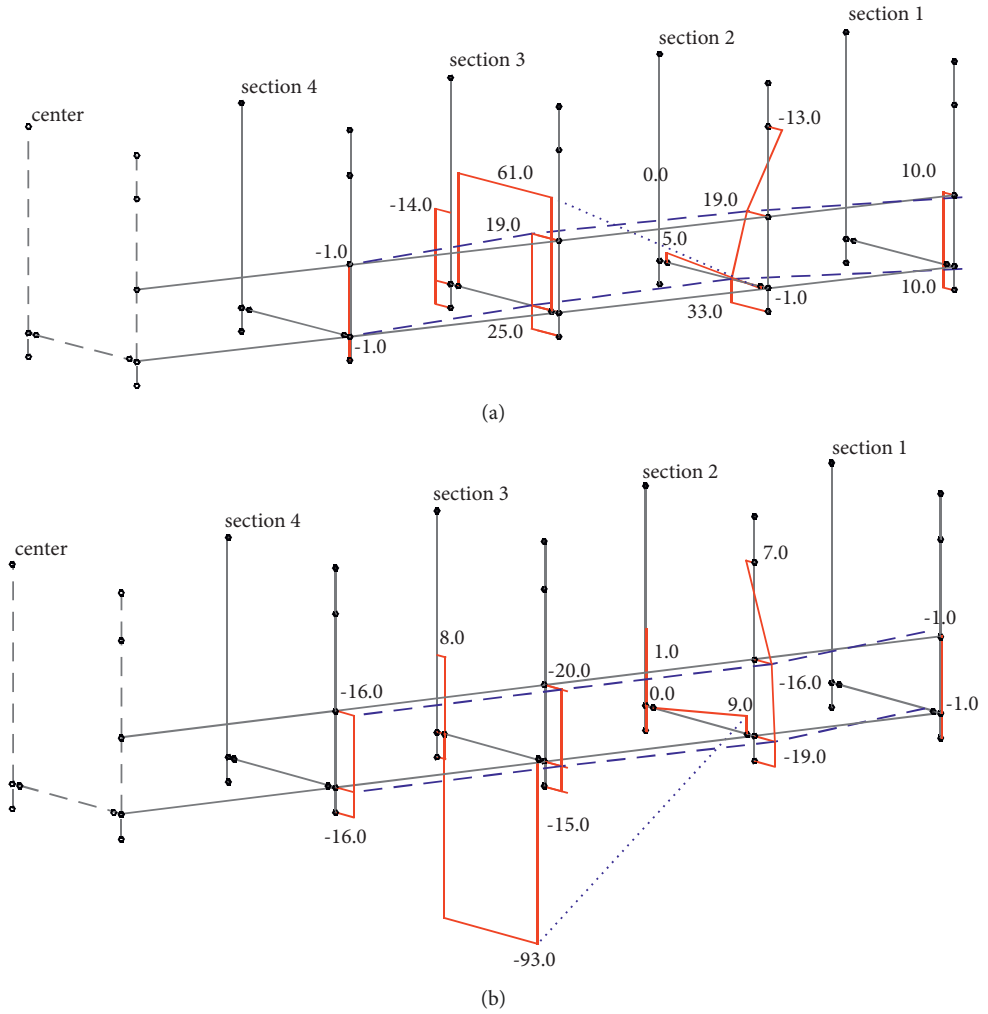

FIGURE 10: Pressure distribution at the time instant of extremes in P9: (a) at $t = 8.35$ s (maximum value at P9); (b) at $t = 15.53$ s (minimum value at P9).

pressure taps P2 and P3, it is the first one. Finally, for pressure tap P7, the most relevant mode is the fourth one.

As it was expected, the highest value of normalized kinetic energy $\overline{\overline{E_c}}$ (i.e., $\overline{\overline{E_c}} = E_{c,i}/\max(E_{c,i})$) is for the first mode of pressure tap P2 because it is the closest pressure tap in section S2, in the upwave direction. The large values calculated for the 4th mode in P7 and the 2nd mode in P1 suggest that after the truck passage, the pressure induced by the piston effect preserves a non-negligible kinetic energy value.

The pressure distributions illustrated in Figure 8 consist of an envelope of the peak values that do not occur simultaneously. On the contrary, Figure 10 shows the pressure distribution at two different time instants, $t = 8.35$ s and 15.53 s, linked with the occurrence of maxima and minima values at the pressure tap P9. In both cases, these three-dimensional views show a parabolic trend in the vertical direction from P12 to P8 (Figure 4) and a quick decrement in the horizontal direction from P9 to P1 (Figure 4).

Figure 11 gives an overview of pressure maxima and minima that occur step by step on the bridge recorded by pressure taps. Following the maxima and minima trends step by step, referring to Figure 4, the piston and recoil effect were clearly observed.

4.2. Pressure Fields Spatial Correlation. In order to investigate the effect of truck passage-induced wave on all of the considered surfaces of the bridge, the correlation coefficients (ϕ) between the entire pressure records were calculated [15]. Their values are given in Table 4. The largest value for each pressure tap is marked in bold (value 1 means the auto-correlation). As it was expected, significant correlations are observed between P2 and P3 and between P10 and P11 that are close together (Figure 4). However, despite the expectations, quite small value of the correlation coefficient was observed between P1 and P7 that are in line in section S2 (Figure 4). It is reasonable to conclude that the flow

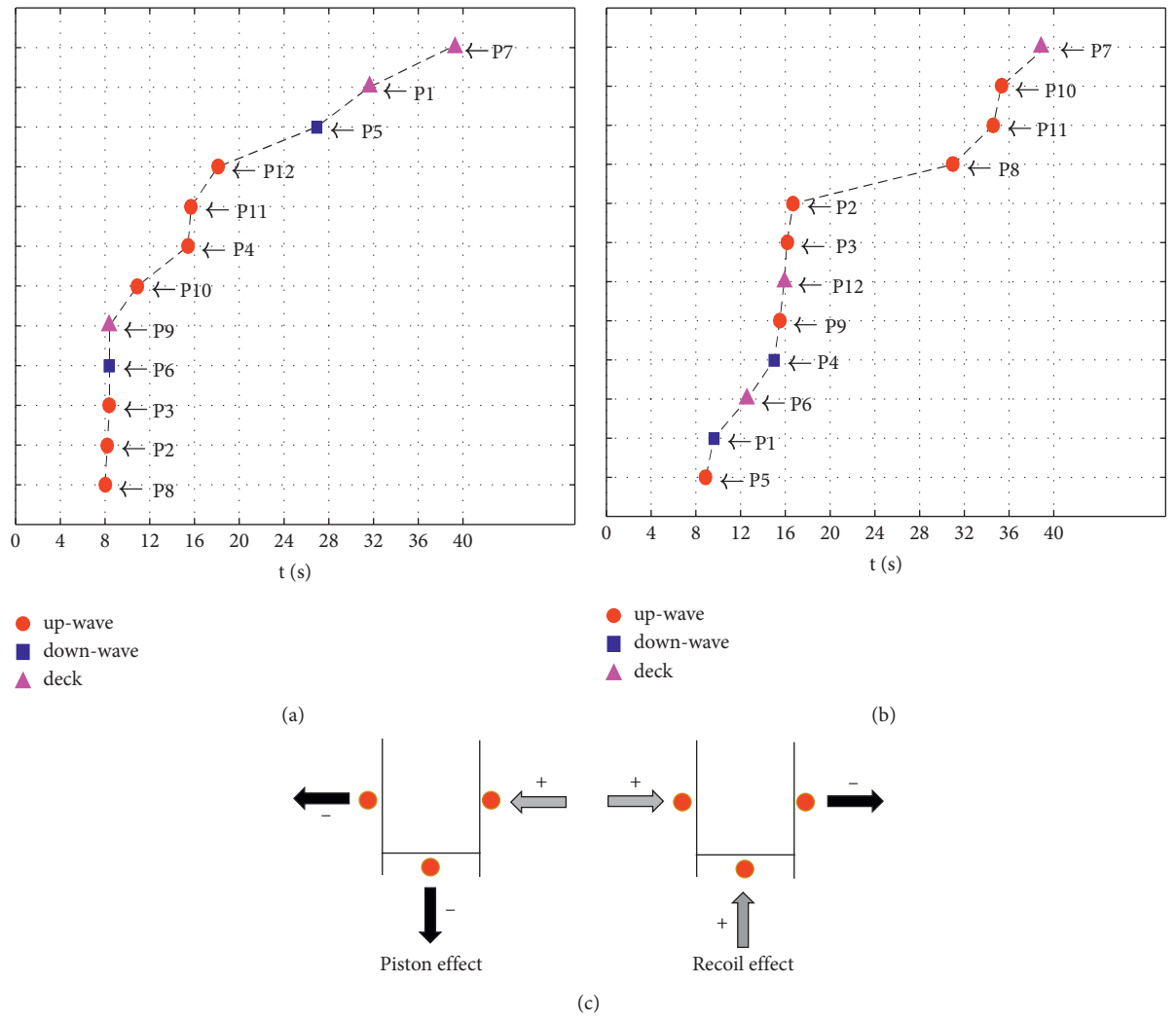

Figure 11: Pressure maxima (a) and minima (b) on the bridge, step by step.

Table 4: Pressure series correlation coefficients ($t = 60$ s).

ϕ	P1	P2	P3	P4	P5	P6	P7	P8	P9	P10	P11	P12
P1	1.00	0.09	0.20	0.08	0.39	0.37	0.22	0.20	0.52	0.25	0.07	0.01
P2	0.09	1.00	0.46	0.08	0.04	0.15	0.19	0.17	0.13	0.07	0.22	0.10
P3	0.20	**0.46**	1.00	0.04	0.18	0.03	0.23	0.24	0.02	0.08	0.03	0.29
P4	0.08	0.08	0.04	1.00	0.12	0.17	0.04	0.21	0.20	0.07	0.07	0.09
P5	**0.39**	0.04	0.18	0.12	1.00	0.18	0.32	0.03	0.09	0.16	0.13	0.15
P6	**0.37**	0.15	0.03	0.17	0.18	1.00	0.18	0.17	0.13	0.10	0.18	0.13
P7	0.22	0.19	0.23	0.04	**0.32**	0.18	1.00	0.13	0.24	0.14	0.03	0.10
P8	0.20	0.17	**0.24**	0.21	0.03	0.17	0.13	1.00	0.11	0.15	0.05	0.16
P9	**0.52**	0.13	0.02	0.20	0.09	0.13	**0.24**	0.11	1.00	0.20	0.12	0.09
P10	0.25	0.07	0.08	0.07	0.16	0.10	0.14	0.15	0.20	1.00	0.55	0.02
P11	0.07	0.22	0.03	0.07	0.13	0.18	0.03	0.05	0.12	**0.55**	1.00	0.10
P12	0.01	0.10	0.29	0.09	0.15	0.13	0.10	0.16	0.09	0.02	0.10	1.00

Bolded values mean peaks.

detachment occurred, and the consequent flow separation have induced different pressure streamlines under the deck.

The correlation coefficient between P1 and P9 is also significant, and it seems to disprove the trend illustrated in Figure 10 where it is shown that the maxima or minima values in P9 (section 3) correspond to very small pressure values in P1. The small correlation coefficients correspond to quite a different power spectral density (PSD), as it is illustrated in Figure 12.

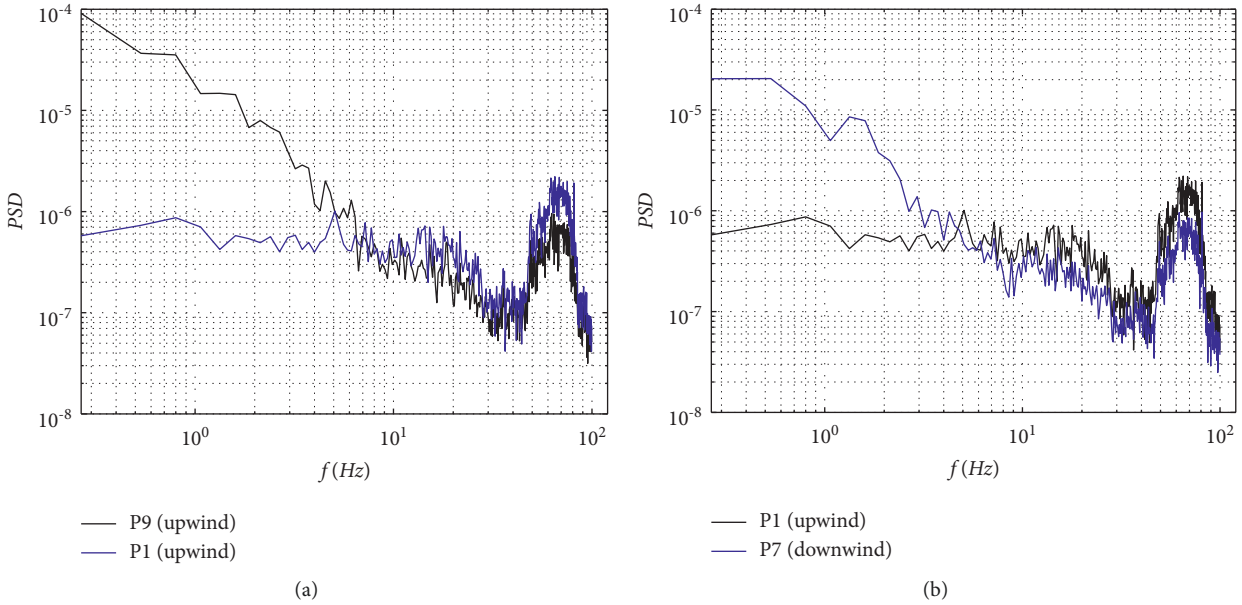

Figure 12: Power spectral density of processes recorded by P1 and P9 (a) and P1 and P7 (b).

This figure provides a comparison between the power spectral density of processes recorded by P1 and P9 (Figure 12(a)) and P1 and P7 (Figure 12(b)).

4.3. Accelerations under the Truck Passage. The monitoring campaign included measurements from six accelerometers which were used to identify the dynamics of the structure, and the measured signals are illustrated in Figure 13. Aliasing phenomena due to noise were filtered from accelerometer measurements using a quadratic Butterworth bandpass 4th order filter with 0.1 Hz and 20 Hz as lower and upper cutoff frequencies.

Table 5 gives the maxima and minima values of accelerations (a) at the instant t, for both upwave and downwave sides (Figure 5). In this paper, negative acceleration values mean $v_{1(t)>}v_{0(t)}$ according to

$$a_{(t)} = \frac{v_{1(t)-}v_{0(t)}}{t_1 - t_o}, \quad (t_1 - t_o) > 0. \tag{2}$$

The highest peak of acceleration was recorded by using an accelerometer A5 upwave (i.e., negative value). Upwave positive accelerometric values ranged from 0.087 m/s^2 to 0.24 m/s^2 with the maximum in A5 (section 5). Negative values ranged from −0.3 m/s^2 to −0.13 m/s^2. The minimum, as expected, was observed in A5 (section 5), as this section was located in the middle span of the bridge.

The downwave maxima vary between 0.16 m/s^2 (section 2, A4) and 0.26 m/s^2 at the support (section 0, A2). The minima are practically constant for all accelerometers. Except for accelerometer A3 and A5 that measured the maximum value in the first 2-3 seconds, the instants of the maxima are in the range between 12.49 and 57.41 s.

The difference between upwave and downwave values of accelerations suggests a different vibration between upwave and downwave sides during truck passage. The reinforced concrete deck plate ensures the reliability and safety of the structure after its construction. However, without the reinforced concrete plate, some geometrical imperfections can induce unexpected effects, e.g., misalignment at supports or rotation of beams around their axes, and this can occur during the bridge construction.

It was observed that, overall, pressure and acceleration peaks are not simultaneous, and this may be accounted to the bridge aerodynamics that induce a random vortex shedding and consequently, a different vibration in different parts of the bridge.

The first two structural frequencies (f_t) under the wave are estimated using a standard fast Fourier transform (FFt), and their amplitudes are shown in Figure 14 for all of the measured signals. Two clear peaks can be observed around 1.9 Hz and 4.9 Hz that correspond to the first vertical and the first torsional modal frequencies, respectively. Through a finite element method (FEM) analyses by the software MIDAS [16], a numerical model was calibrated to simulate the modal frequencies under wave. The modal analysis was repeated by eliminating the reinforced concrete plate, and it was observed that values of the first vertical mode frequency and the first torsional mode frequency were equal to 2.3 Hz and 2.9 Hz, respectively. It was also observed that frequencies are very close to the pedestrian pacing frequency, according to values given by Newl [17], and published by Bachmann and Ammann [18], that are about 1.7 Hz and 3.2 Hz, for a slow walk and for fast running, respectively.

Figure 15 shows the deformed modal shapes with and without the reinforced concrete plate. The first torsional mode frequency without the reinforced concrete plate is about 60% smaller than with the reinforced concrete plate, which is in compliance with the significant vibrations under the truck passage waves measured during the construction without the concrete deck. On the contrary, the first vertical mode frequency increases of about 20% and it comes close to the

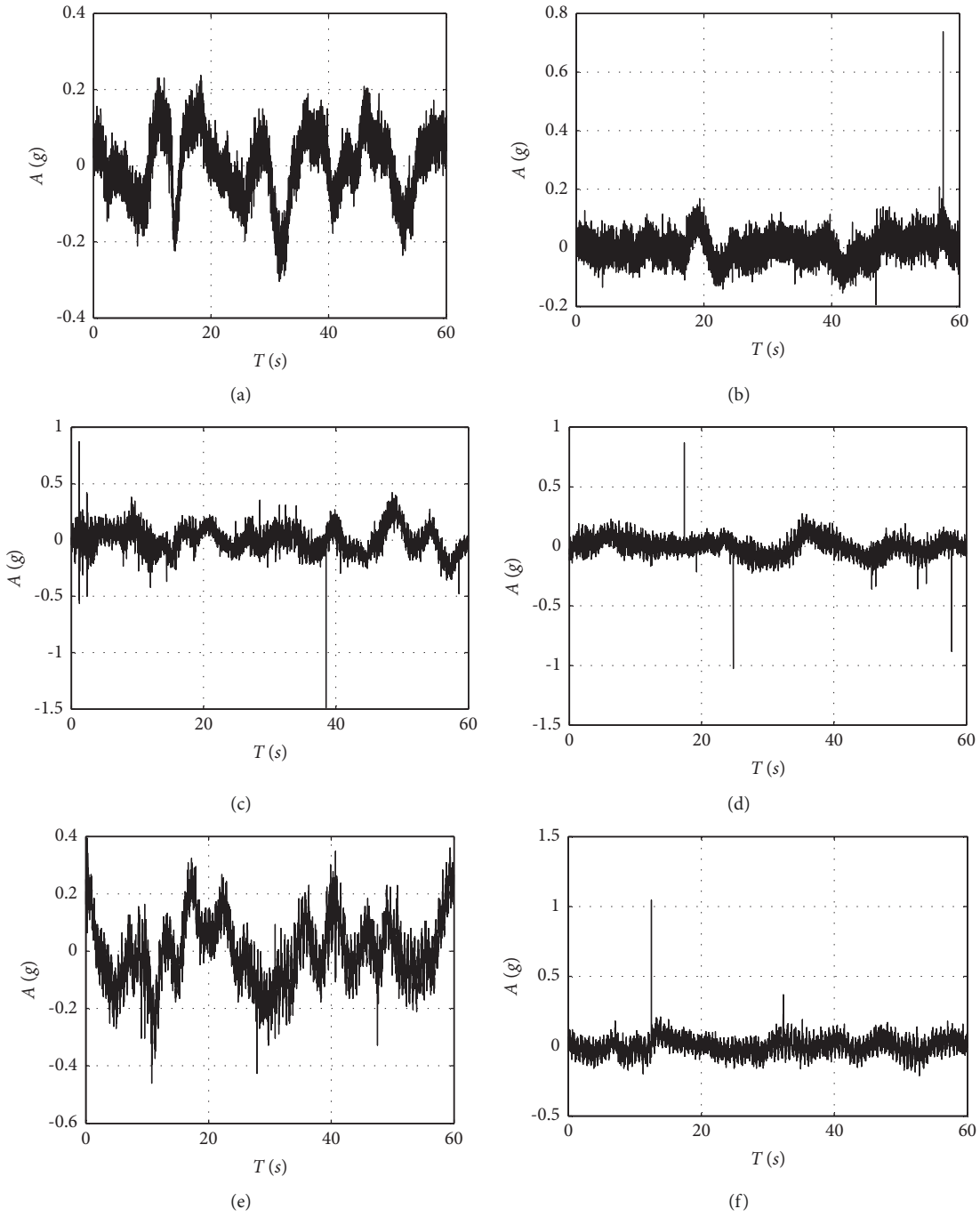

Figure 13: Accelerations recorded at A1 (a), A2 (b), A3 (c), A4 (d), A5 (e), and A6 (f).

Table 5: Extreme values and instants of acceleration measurements.

Position	Section	Sensor	Max		Min	
			a (m/s^2)	t (s)	a (m/s^2)	t (s)
Upwave	0	A1	0.087	18.27	−0.130	31.60
	2	A3	0.110	1.18	−0.130	38.52
	5	A5	0.240	0.20	−0.300	10.76
Downwave	0	A2	0.260	17.40	−0.140	24.78
	2	A4	0.160	57.41	−0.160	46.93
	5	A6	0.190	12.49	−0.180	52.78

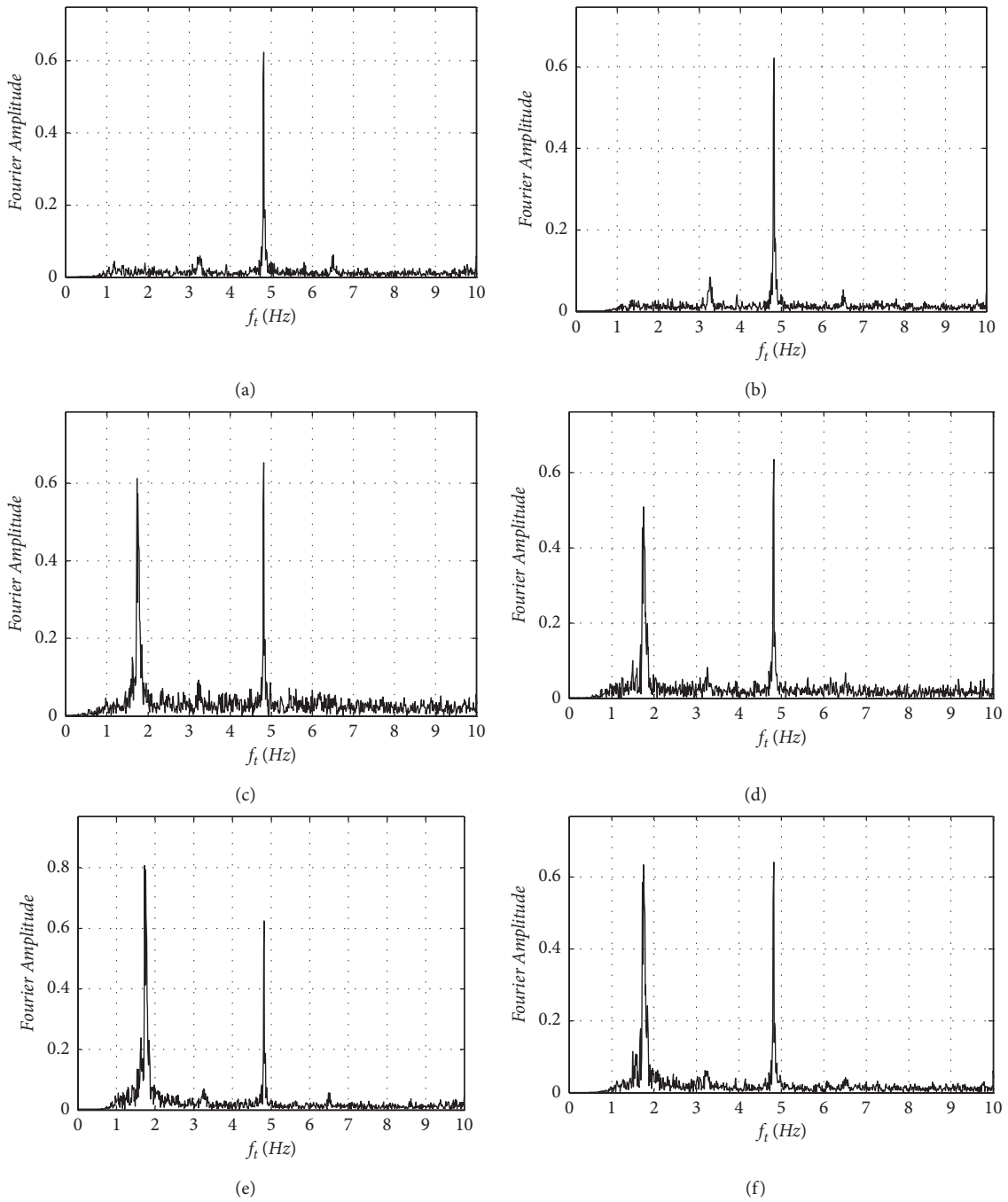

Figure 14: Fourier amplitude accelerations A1 (a), A2 (b), A3 (c), A4 (d), A5 (e), and A6 (f).

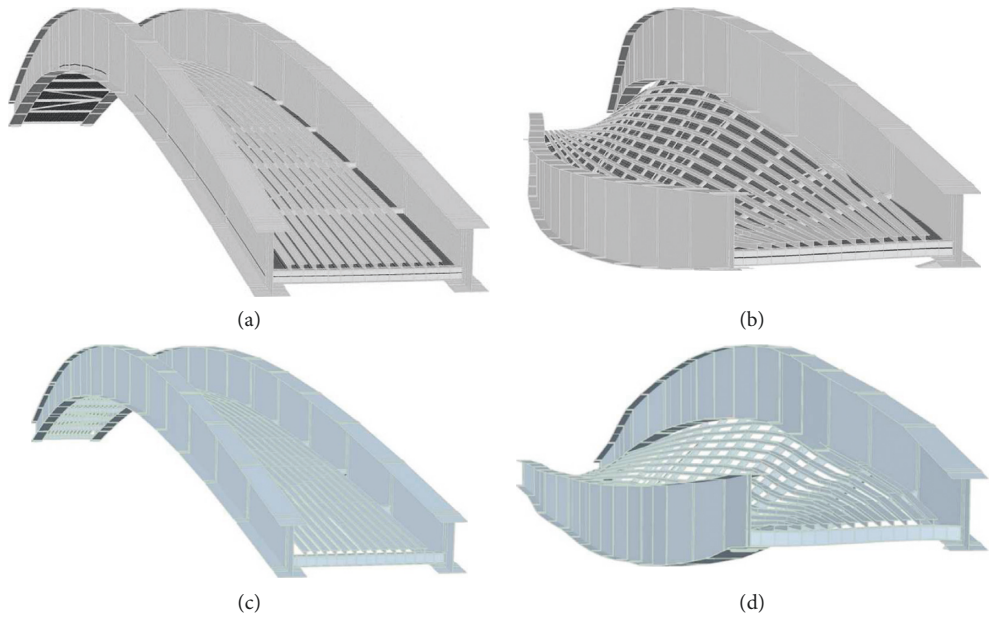

Figure 15: Significant modal shapes of the Pregnana footbridge: (a) first vertical mode, (b) first torsional mode; Pregnana footbridge without concrete deck: (c) first vertical mode, (d) first torsional mode.

torsional frequency. In conclusion, it was observed that the reinforced concrete plate improves the structural torsional stiffness, but its mass negatively affects the vertical stiffness.

5. Conclusions

This paper discusses the interaction between the truck passage-induced waves and a pedestrian bridge through results of an experimental campaign. Pressure and accelerometric signals acquired during truck passage have shown that airwaves expand parabolically along the longitudinal sides of the bridge, from the center to the supports. Results also show that the maximum pressures occurred under the bridge and that these values are comparable with the values of pressure suggested for train passage under bridges. It was observed that the bridge torsional and vertical modes vary significantly with and without the reinforced concrete plate on the deck and analyses strongly suggest the use of a rigid deck to avoid undesired vibrations under the truck passage and the piston effect. Analyses suggest that the piston effect should be calculated to safely construct light bridges. This paper can be considered a starting point of the investigation of the piston effect, which can have a significant structural impact on light pedestrian bridges above highways. Further investigations are necessary to collect more data in order to formulate guidelines and standards on the design procedures regarding dealing with this effect in practice.

Data Availability

The data will be available by email if requested.

Conflicts of Interest

The authors declare that they have no conflicts of interest.

References

[1] I. P. T. Firth, *New Materials for Modern Footbridges*, AFGC & OTUA Footbridge, Paris, France, 2002.

[2] C. Bojanowski, S. A. Lottes, and M. A. Sitek, *CFD Estimation of Truck Induced Wind Gusts on Variable Message Signs*, Nuclear Science and Engineering Division National Technical Information Service (NTIS), 2009.

[3] P. Zółtowski, J. Piechna, K. Zółtowski, and H. Zobel, "Analysis of dynamic loads on lightweight footbridge caused by truck passing underneath," *Bulletin of the Polish Academy of Sciences, Technical Sciences*, vol. 54, no. 1, 2006.

[4] R. McCallen, F. Browand, and J. Ross, *The Aerodynamics of Heavy Vehicles: Trucks*, Buses and Trains, Eds., Springer Berlin Heidelberg, New York, 2004.

[5] S. Pan, L. Fan, J. Liu et al., "A review of the piston effect in subway stations," *Advances in Mechanical Engineering*, vol. 2013, Article ID 950205, 2013.

[6] M. B. Creamer, K. H. Frank, and R. E. Klinger, "Fatigue loading of cantilever sign structures from truck wind gusts," *Center for Highway Research*, Technical report, The University of Texas at Austin, Austin, Texas 78712, 1979.

[7] K. W. Johns and R. J. Dexter, "The development of fatigue design load ranges for cantilevered sign and signal support structures," *Journal of Wind Engineering and Industrial Aerodynamics*, vol. 77-78, pp. 315–326, 1998.

[8] M. S. Gallow, *Mitigating Fatigue of Cantilevered Overhead Sign Structures Due to Natural and Truck-Induced Wind Gusts*, Master of Science in Civil Engineering thesis, University of Alabama at Birmingham, Birmingham, Alabama, 2014.

[9] "CEN (comité européen de Normalization)," 2005, https://www.cencenelec.eu/.

[10] M. Petrangeli and A. Viskovic, "Torsional behaviour in beam and slab decks," in *Proceedings of the 7th Int. Conf. on Short & Medium Span Bridges*, pp. 23–25, IABSE, Montréal, Aug 2006.

[11] M. Petrangeli, G. Usai, F. Magnorfi, M. Orlandini, and M. Pietrantoni, "Il nodo di Pregnana," *Le Strade, in itailian*, vol. 1447, pp. 158–166, 2009.

[12] K. S. Kumar and T. Stathopoulos, "Wind loads on low building roofs: a stochastic perspective," *Journal of Structural Engineering*, vol. 126, no. 8, pp. 944–956, 2000.
[13] "Rete ferroviaria italiana (RFI)," technical report, 2005.
[14] Y. Tamura, S. Suganuma, H. Kikuchi, and K. Hibi, "Proper orthogonal decomposition of random wind pressure field," *Journal of Fluids and Structures*, vol. 13, no. 7-8, pp. 1069–1095, 1999.
[15] F. Rizzo, V. Sepe, F. Ricciardelli, and A. M. Avossa, "Wind pressures on a large span canopy roof," *Wind and Structures*, vol. 30, no. 2, 2020.
[16] "Midas civil manuals and tutorials," https://globalsupport.midasuser.com/helpdesk/KB/View/32609792-midas-civil-manuals-and-tutorials.
[17] D. E. Newl, "Pedestrian excitation of bridges," *Proceedings of the Institution of Mechanical Engineers - Part C: Journal of Mechanical Engineering Science*, vol. 218, no. 5, pp. 477–492, 2004.
[18] H. Bachmann and W. Ammann, "Vibrations in structures induced by man and machines," *IABSE Structural Engineering Document 3e*, International Association for Bridge and Structural Engineering, ürich, Switzerland, 1987.